



Nonlinear coupled moving-load excited dynamics of beam-mass structures

M. H. Ghayesh¹ · H. Farokhi² · Y. Zhang¹ · A. Gholipour¹

Received: 12 February 2020 / Revised: 24 February 2020 / Accepted: 3 March 2020 / Published online: 6 April 2020
© Wrocław University of Science and Technology 2020

Abstract

Investigated in this paper is the first on the moving-load-caused nonlinear coupled dynamics of beam-mass systems. A constant value load excites the beam-mass system where its position on the beam-mass system changes periodically. The energy contribution of the moving load is included via a virtual work formulation. The kinetic energy of the mass together with the beam as well as energy stored in the beam after deflection is formulated. Hamilton's principle gives nonlinear equations of the beam-mass system under a moving load in a coupled transverse/longitudinal form. A weighted-residual-based discretisation gives a 20 degree of freedom which is numerically integrated via continuation/time integration along with Floquet theory techniques. The resonance dynamics in time, frequency, and spatial domains is investigated. As we shall see, torus bifurcations are present for some beam-mass structure parameters as well as travelling waves. A finite element analysis is performed for a simpler linear version of the problem for to-some-extend verifications.

Keywords Moving load · Beam-mass structure · Nonlinear dynamics · Stability · Bifurcation

1 Introduction

Plates, beams, and shells as the most famous continuous structures can be found as building blocks of many mechanical/civil systems; Polus and Szumigala [1] analysed aluminium–concrete composite beams using a three-dimensional finite element technique and found very good agreement between experiments and theory. Domagalski [2] considered periodically inhomogeneous beams and examined the vibration behaviour in the absence of loadings and subject to external loadings via the Galerkin techniques for frequency–amplitude responses. In some applications, their nonlinear response becomes important. Loads applied to these structures have different natures such as randomly/harmonically varying magnitude. There are also mechanisms where the applied load changes its position; for instance, Mohanti et al. [3] employed a single-mode approximation in the framework of the method of multiple scales in the

presence of a moving mass and obtained the corresponding time histories. One famous application is in bridges, where the moving cars and passengers could be considered as moving loads and depending on the value and sequence of them the dynamics could be analysed.

For a supported–supported beam-mass system, a geometric type of nonlinearity due to stretching influences becomes important in the nonlinear dynamical behaviour. Another feature is the couplings of linear/nonlinear type between the transverse/longitudinal displacements/inertia; none of these have been ignored in the modelling/simulations.

Investigations into the moving-load-caused dynamics of beams may be categorised into linear and nonlinear. In the first class, the geometric nonlinearity is assumed to be small for near-equilibrium dynamics; for instance, Dimitrovova [4] formulated a viscoelastically supported beam subject to a moving harmonic load using the Bernoulli–Euler theory and developed a semi-analytical solution by means of the integral transform and contour integration methods. Esen [5] used a modified version of the finite element technique for the linear dynamics analysis of functionally graded Timoshenko beams subject to a variable-velocity moving mass and obtained the deflection-velocity curves. Roy et al. [6] considered an infinitely long beam under a uniform-speed harmonically moving force and analysed its dynamics.

✉ M. H. Ghayesh
mergen.ghayesh@adelaide.edu.au

¹ School of Mechanical Engineering, University of Adelaide, Adelaide, SA 5005, Australia

² Department of Mechanical and Construction Engineering, Northumbria University, Newcastle upon Tyne NE1 8ST, UK

Yang and Wang [7] obtained the dynamical behaviour of an inclined beam under a moving vertical force and conducted stability analysis. Yang et al. [8], for bi-directionally graded beams, conducted a dynamic response analysis using a boundary-domain integral equation technique and analysed the natural frequencies and forced vibrations. Sarparast and Ebrahimi-Mamaghani [9] conducted forced/free vibrations analysis due to moving loads on laminated curved beams via the Galerkin method and obtained the fundamental frequency and displacements.

There are a limited number of investigations in the literature which considered *nonlinearities* [2, 10–12]. Correa et al. [13], for an Euler–Bernoulli beam under a moving load, developed a dynamic model using the finite element (FE) model in the presence of non-smooth frictional damping. In a study by Chen et al. [14], the thermo-mechanical dynamic responses of a laminated beam under a harmonically moving force by means of the finite difference method and time histories were obtained. Zupan and Zupan [15] employed a three-dimensional framework for the dynamic analysis of beams with a moving mass through use of a finite element formulation. Khurshudyan and Ohanyan [16] considered a nonlinear Bernoulli–Euler beam excited by two moving loads in opposite directions and analysed the nonlinear vibrations using the Bubnov–Galerkin procedure.

This article is the first to study the moving-load-caused local nonlinear coupled dynamical response of beam-mass systems. Two coupled partial differential equations describing the coupled transverse/longitudinal motion are formulated using a Hamilton-based technique. A load with a constant magnitude with a harmonically changing position excites the beam-mass system. The corresponding work contribution is formulated. Mass kinetic energy together with that of the beam as well as the energy stored in the beam after deflection is formulated. Using Hamilton's principle results in the moving-load-caused nonlinear dynamics model of the beam-mass structure. A 20-DOF system is obtained via a weighted-residual-based discretisation scheme; this is numerically integrated by means of continuation/time-integration techniques. The nonlinear and resonance dynamical behaviour in frequency, time, and spatial domains is investigated. A FEA model is developed for a simple linear version for linear natural frequency verifications.

2 Coupled model for moving-load-caused dynamics of beam-mass structure

As illustrated in Fig. 1, the beam-mass system assembly consists of a straight beam with a mass M attached to it at a distance ξ_M from the left end with the following assumptions:

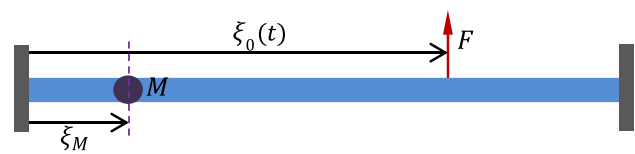


Fig. 1 A beam-mass system with a moving load

- The beam is considered of an Euler–Bernoulli type; hence, the shear deformation/rotary inertia are neglected.
- Large rotations and stretching nonlinearities are considered.
- The motion is considered to be planar.
- The beam is considered perfectly straight.
- The mass is assumed to be a point mass; hence, there are no rotary inertia influences.
- The mass is attached to the centreline of the beam.
- A Lagrangian system of movement description is used.
- The beams is considered to be homogenous with uniform properties.
- The moving load is considered as a point force.

EI , EA , L , and A are the flexural rigidity, axial stiffness, length, and cross-sectional area of the beam, respectively. m is beam's mass per unit length. A constant-magnitude moving point force F is applied to the beam whose distance from the left end, $\xi_0(t)$, is given by

$$\xi_0(t) = \frac{L}{2}(1 - s_f \cos(\omega_f t)), \quad (1)$$

where ω_f is the frequency of the position change and s_f is a parameter determining the boundaries of the position of the moving load. The virtual work of this moving load is given by

$$\delta W_F = \int_0^L F \delta_{\text{Dirac}}(\xi - \xi_0(t)) \delta \chi_2 d\xi, \quad (2)$$

where χ_2 is the displacement in transverse direction.

Defining χ_1 as the displacements in axial direction and ρ as the centreline rotation, the strain term (incorporating both stretching and curvature nonlinearities) can be written as [17]

$$\varepsilon_{\xi\xi}(t, \xi, z) = \sqrt{\left(\frac{\partial \chi_1(t, \xi)}{\partial \xi} + 1\right)^2 + \left(\frac{\partial \chi_2(t, \xi)}{\partial \xi}\right)^2} - 1 - z \frac{\partial \rho(t, \xi)}{\partial \xi}, \quad (3)$$

resulting in the potential energy of the beam as [18]

$$\delta U = \int_0^L \int_A E \left[\sqrt{\left(\frac{\partial \chi_2(t, \xi)}{\partial \xi}\right)^2 + \left(\frac{\partial \chi_1(t, \xi)}{\partial \xi} + 1\right)^2} - 1 - \left(\frac{\partial \rho(t, \xi)}{\partial \xi}\right) z \right] \times \delta \left[\sqrt{\left(\frac{\partial \chi_2(t, \xi)}{\partial \xi}\right)^2 + \left(\frac{\partial \chi_1(t, \xi)}{\partial \xi} + 1\right)^2} - 1 - \left(\frac{\partial \rho(t, \xi)}{\partial \xi}\right) z \right] dA d\xi. \tag{4}$$

Defining a linear viscous damping of coefficient c for the motion, the dissipative work is formulated as [19]

$$\delta W_d = - \int_0^L \left(c \left(\frac{\partial \chi_1}{\partial t}\right) \delta \chi_1 + c \left(\frac{\partial \chi_2}{\partial t}\right) \delta \chi_2 \right) d\xi. \tag{5}$$

Formulation of the motion energy gives

$$T = \frac{1}{2} \int_0^L (m + M \delta_{\text{Dirac}}(\xi - \xi_M)) \left(\frac{\partial \chi_1}{\partial t}\right)^2 d\xi + \frac{1}{2} \int_0^L (m + M \delta_{\text{Dirac}}(\xi - \xi_M)) \left(\frac{\partial \chi_2}{\partial t}\right)^2 d\xi. \tag{6}$$

Hamilton’s work/energy principle for Eqs. (2), (4), (5), and (6) gives

$$(1 + \gamma \delta_{\text{Dirac}}(\xi - \xi_M)) \frac{\partial^2 \chi_1}{\partial \tau^2} - \Pi \frac{\partial^2 \chi_1}{\partial \xi^2} - \frac{\Pi}{S} \frac{\partial^2 \chi_2}{\partial \xi^2} \frac{\partial \chi_2}{\partial \xi} - \frac{1}{S} \left(\frac{\partial^3 \chi_2}{\partial \xi^3} \frac{\partial^2 \chi_2}{\partial \xi^2} + \frac{\partial^4 \chi_2}{\partial \xi^4} \frac{\partial \chi_2}{\partial \xi} \right) + c_d \frac{\partial \chi_1}{\partial \tau} = 0, \tag{7}$$

$$(1 + \gamma \delta_{\text{Dirac}}(\xi - \xi_M)) \frac{\partial^2 \chi_2}{\partial \tau^2} + \frac{\partial^4 \chi_2}{\partial \xi^4} + c_d \frac{\partial \chi_2}{\partial \tau} - f_m \delta_{\text{Dirac}} \left[\xi - \frac{1}{2} (1 - s_f \cos(\Omega_f \tau)) \right] - \frac{\Pi}{S} \left(\frac{3}{2S} \left(\frac{\partial \chi_2}{\partial \xi}\right)^2 \frac{\partial^2 \chi_2}{\partial \xi^2} + \frac{\partial \chi_2}{\partial \xi} \frac{\partial^2 \chi_1}{\partial \xi^2} + \frac{\partial \chi_1}{\partial \xi} \frac{\partial^2 \chi_2}{\partial \xi^2} - \frac{1}{S} \left(2 \frac{\partial \chi_1}{\partial \xi} \frac{\partial^4 \chi_2}{\partial \xi^4} + 4 \frac{\partial^2 \chi_1}{\partial \xi^2} \frac{\partial^3 \chi_2}{\partial \xi^3} + \frac{\partial^4 \chi_1}{\partial \xi^4} \frac{\partial \chi_2}{\partial \xi} + 3 \frac{\partial^3 \chi_1}{\partial \xi^3} \frac{\partial^2 \chi_2}{\partial \xi^2} + \frac{1}{S} \left\{ 2 \left(\frac{\partial^2 \chi_2}{\partial \xi^2}\right)^3 + 8 \frac{\partial^2 \chi_2}{\partial \xi^2} \frac{\partial \chi_2}{\partial \xi} \frac{\partial^3 \chi_2}{\partial \xi^3} + 2 \frac{\partial^4 \chi_2}{\partial \xi^4} \left(\frac{\partial \chi_2}{\partial \xi}\right)^2 \right\} \right) = 0, \tag{8}$$

in which the following non-dimensionalisations have been performed

$$\langle \xi^*, \xi_M^*, \chi_1^*, \chi_2^*, S \rangle = \left\langle \frac{\xi}{L}, \frac{\xi_M}{L}, \frac{\chi_1}{h}, \frac{\chi_2}{h}, \frac{L}{h} \right\rangle, \tag{9}$$

$$\Omega_f = \omega_f L^2 \sqrt{\frac{m}{EI}}, \tau = \frac{t}{L^2} \sqrt{\frac{EI}{m}},$$

$$c_d = \frac{cL^2}{EI} \sqrt{\frac{EI}{m}}, \Pi = \frac{AL^2}{T}, f_m = \frac{FL^2}{EIh}, \gamma = \frac{M}{mL}$$

and the asterisk is dropped for brevity.

One way of dealing with Eqs. (7) and (8), which are complex/coupled in nonlinear ways, and solving them together for time/frequency domains is to discretise them; however, it is important to retain enough number of discretisation terms (here 20 modes) to get reliable/converged results; in a non-linear sense, this makes numerical integrations expensive and time-consuming. So, defining series expansion of

$$\begin{bmatrix} \chi_1 \\ \chi_2 \end{bmatrix} = \sum_{k=1}^{10} \begin{bmatrix} (r_k(\tau) \Delta_k(\xi)) \\ (\Gamma_k(\xi) p_k(\tau)) \end{bmatrix}, \tag{10}$$

with

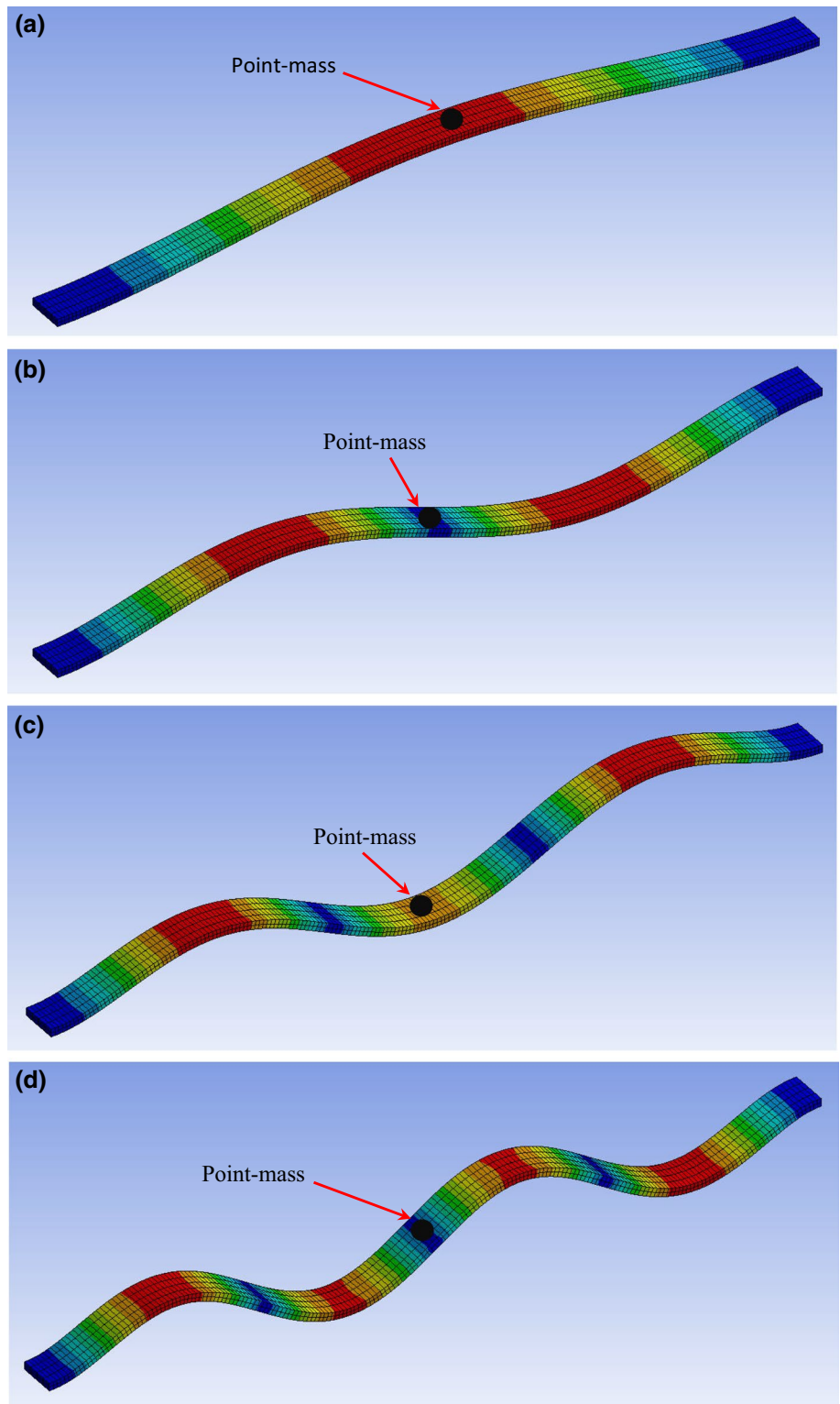
$$\begin{bmatrix} \Delta_k \\ \Gamma_k \end{bmatrix} = \begin{bmatrix} (\sin(k\pi\xi)) \\ [-\cos(\alpha_k\xi) + \theta_k \sin(\alpha_k\xi) - [\theta_k \sinh(\alpha_k\xi) - \cosh(\alpha_k\xi)]] \end{bmatrix}$$

$$\theta_k = (\sinh \alpha_k - \sin \alpha_k)^{-1} (\cosh \alpha_k - \cos \alpha_k) \tag{11}$$

and weakening Eqs. (7) and (8) via a weighted-residual approach gives

$$\left. \begin{aligned} \dot{r}_k &\leftrightarrow \sum_{j=1}^{10} \left[\int_0^1 \Delta_j \Delta_k (1 + \gamma \delta_{\text{Dirac}}(\xi - \xi_M)) d\xi \right] \\ \dot{r}_k &\leftrightarrow +c_d \sum_{j=1}^{10} \left(\int_0^1 \Delta_j \Delta_k d\xi \right) \\ r_k &\leftrightarrow -\Pi \sum_{j=1}^{10} \left(\int_0^1 \Delta_k'' \Delta_j d\xi \right) \\ p_k p_l &\leftrightarrow -\frac{\Pi}{S} \sum_{k=1}^{10} \sum_{l=1}^{10} \left(\int_0^1 \Delta_j \Gamma_k'' \Gamma_l' d\xi \right) - \frac{1}{S} \sum_{k=1}^{10} \sum_{l=1}^{10} \left[\int_0^1 (\Gamma_k''' \Gamma_l'' + \Gamma_k'''' \Gamma_l') \Delta_j d\xi \right] = 0 \\ j &= 1, 2, \dots, 10 \end{aligned} \right\} \tag{12}$$

Fig. 2 FEA free linear dynamics with point mass: first four mode shapes



$$\left. \begin{aligned}
 \ddot{p}_k &\leftrightarrow \sum_{k=1}^{10} \left(\int_0^1 (1 + \gamma \delta_{\text{Dirac}}(\xi - \xi_M)) \Gamma_k \Gamma_j d\xi \right) \\
 \dot{p}_k &\leftrightarrow +c_d \sum_{k=1}^{10} \left(\int_0^1 \Gamma_k \Gamma_j d\xi \right) \\
 p_k &\leftrightarrow + \sum_{k=1}^{10} \left(\int_0^1 \Gamma_k'''' \Gamma_j d\xi \right) \\
 r_k p_l &\leftrightarrow -\frac{\pi}{S} \sum_{k=1}^{10} \sum_{l=1}^{10} \left(\int_0^1 [\Delta_k' \Gamma_l'' + \Delta_k'' \Gamma_l'] \Gamma_j d\xi \right) - \frac{1}{S} \sum_{k=1}^{10} \sum_{l=1}^{10} \left(\int_0^1 [2\Delta_k' \Gamma_l'''' + \Delta_k'''' \Gamma_l' + 4\Delta_k'' \Gamma_l'' + 3\Delta_k'''' \Gamma_l'] \Gamma_j d\xi \right) p_k p_l \\
 p_k p_l p_m &\leftrightarrow -\frac{1}{S^2} \sum_{k=1}^{10} \sum_{l=1}^{10} \sum_{m=1}^{10} \left(\int_0^1 [2\Gamma_k'''' \Gamma_l' \Gamma_m' + 2\Gamma_k'' (\Gamma_l'' \Gamma_m'' + 4\Gamma_l' \Gamma_m''')] \Gamma_j d\xi \right) p_k p_l p_m \\
 &\quad - \frac{3}{2} \frac{\pi}{S^2} \sum_{k=1}^{10} \sum_{l=1}^{10} \sum_{m=1}^{10} \left(\int_0^1 \Gamma_k'' \Gamma_l' \Gamma_m' \Gamma_j d\xi \right) - f_m \left(\int_0^1 \delta_{\text{Dirac}} \left[\xi - \frac{1}{2} (1 - s_f \cos(\Omega_f \tau)) \right] \Gamma_j d\xi \right) = 0 \\
 j &= 1, 2, \dots, 10
 \end{aligned} \right\} \tag{13}$$

Solving this coupled set of 20 nonlinear equations using a continuation/time-integration technique along with Floquet theory for stability gives time histories as well as force/frequency diagrams and determines stability and bifurcation types. As this procedure is time-consuming and computationally expensive, the computer codes foreach to be well optimised regarding run-times and cores required.

3 Verifications for linear free dynamics

Before proceeding with the coupled/nonlinear results, a linear FEA free dynamics model is developed in ANSYS® (version 19.0, ANSYS Inc., Canonsburg, PA, USA) by keeping the point mass; for the linear system parameters in Sect. 4, the FEA gives the fundamental frequency of $\omega_1 = 21.4519$ which when compared to $\omega_1 = 21.3204$ shows the error percentage of 0.6. The mode shapes are also presented in Fig. 2 for the first four ones.

4 Frequency/time domain dynamics

The frequency/time domain dynamics of a beam-mass structure of length-to-thickness ratio of 100 is examined in this section. The damping ratio of $\zeta = 0.01$ is selected; ω_1 is the first non-dimensional natural frequency. For all cases, $\xi_M = 0.5$. In Figs. 3, 6, 8, 9, 10, and 11, dashed and solid line styles indicate unstable and stable periodic responses, respectively.

For $f_m = 10.0$, $\gamma = 0.04$, and $s_f = 1.0$, the frequency–amplitude diagrams in the moving-load-caused nonlinear resonance of the beam-mass structure are shown in Fig. 3, where (a) shows frequency–amplitude of the transverse motion and (b) that of axial one. The fundamental natural frequency of $\omega_1 = 21.3204$ is obtained for the transverse motion. It is interesting that a nonlinear resonance of hardening type for transverse/longitudinal motions is observed when the

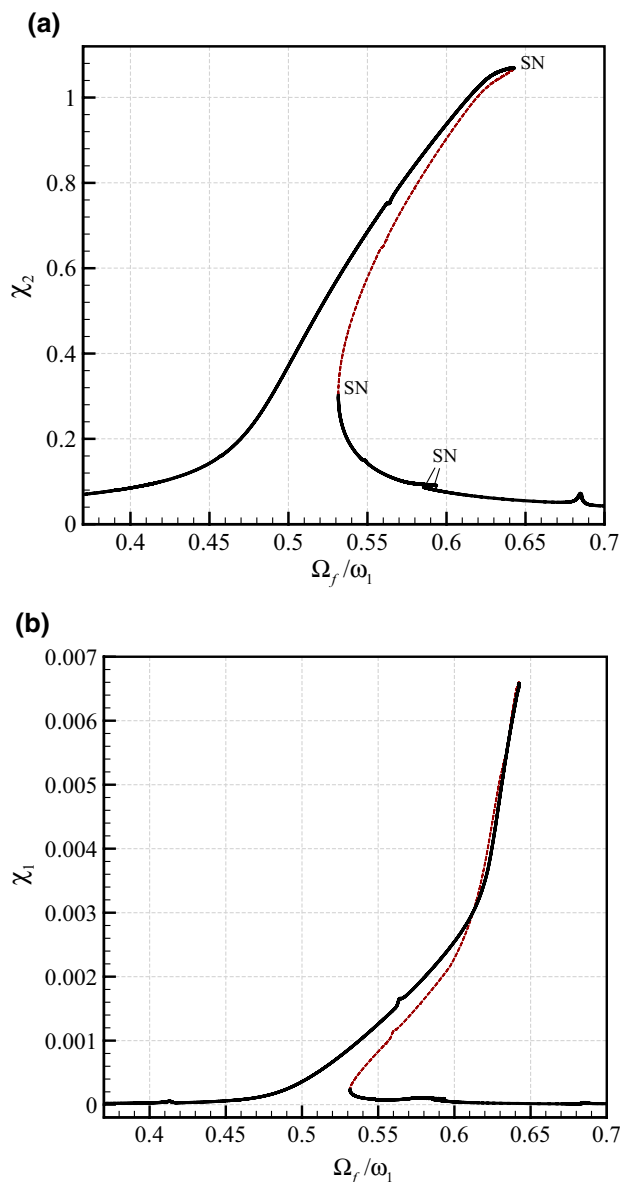


Fig. 3 Frequency–amplitude diagrams of the moving-load excited beam; **a** maximum χ_2 at $\xi = 0.5$; **b** maximum χ_1 at $\xi = 0.66$. $f_m = 10.0$, $\gamma = 0.04$, $s_f = 1.0$, $\omega_1 = 21.3204$

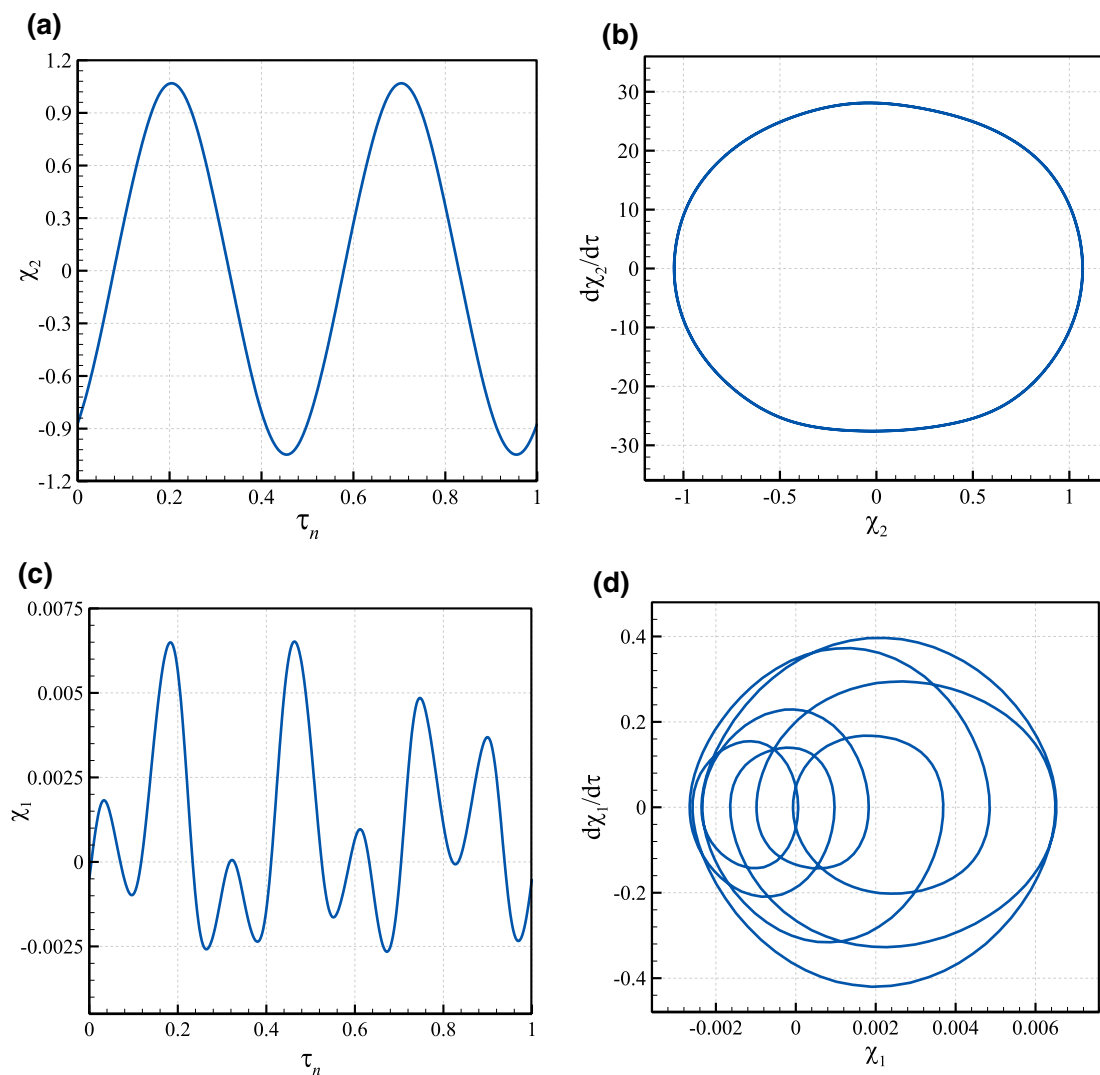


Fig. 4 Motion details for Fig. 2 at $\Omega_f/\omega_1=0.6422$ (which is peak amplitude). **a, b** Time response and phase plane of χ_2 at $\xi=0.5$, respectively; **(c, d)** those of χ_1 at $\xi=0.66$, respectively. τ_n indicates time normalised by oscillation period

frequency of the force position approaches half of beam-mass’s fundamental frequency. Apart from the main saddle-node bifurcation points (at $\Omega_f/\omega_1=0.6425$ and 0.5315), there are two small-amplitude ones in the vicinity of $\Omega_f/\omega_1=0.59$. Highlighted in Fig. 4 are the time response and phase plane of the motion beam-mass system at peak oscillation amplitude, showing the complexity of the longitudinal motion due to nonlinear couplings. The spatial domain distribution of the motion at its largest amplitude is shown in Fig. 5, highlighting the fact of symmetry-breaking and travelling-type motion for the moving-load excited system.

Another interesting aspect of the nonlinear dynamic characteristics of the beam-mass system under a moving load is shown in Fig. 6, highlighting the presence of modal interactions and internal resonances. As seen, as a result of strong

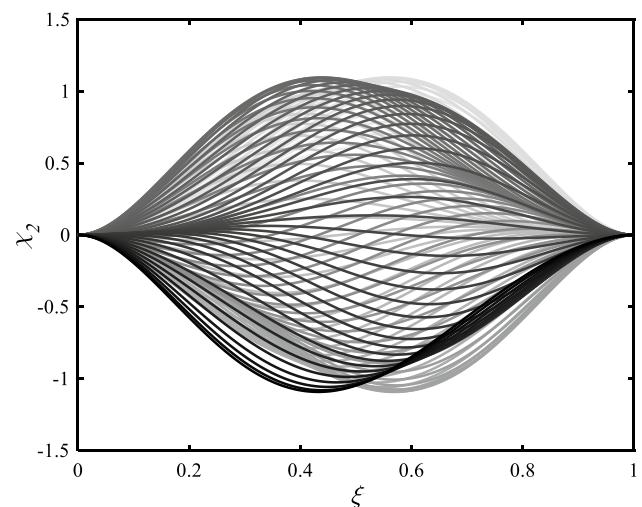


Fig. 5 Transverse moving-load-caused dynamics of the beam-mass structure of Fig. 3 in one period at $\Omega_f/\omega_1=0.6422$

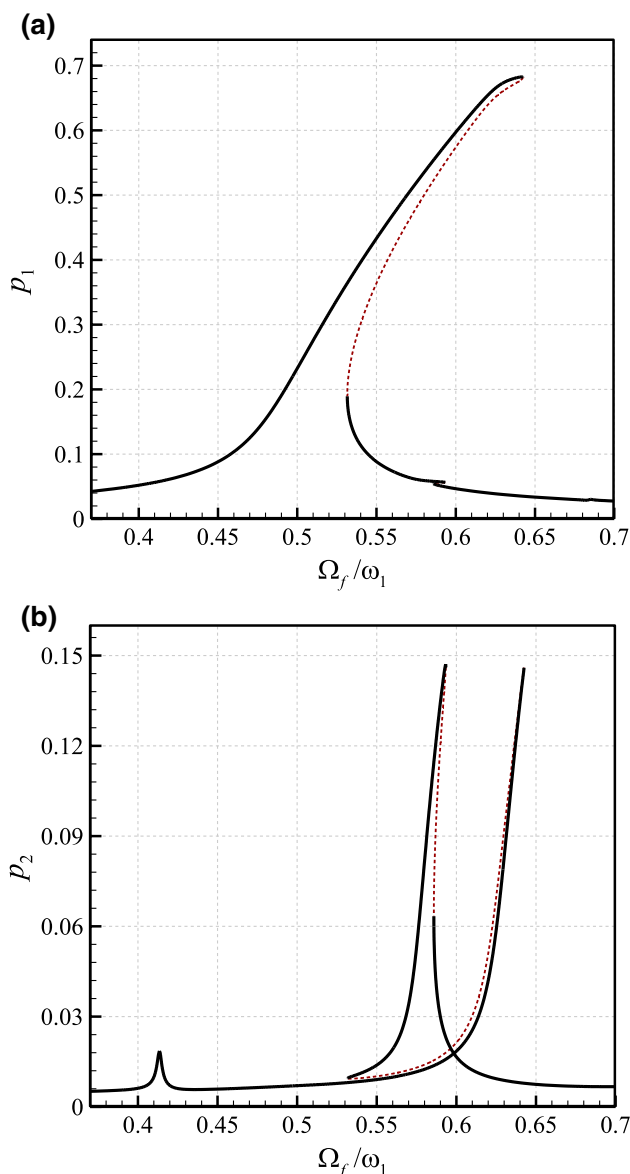


Fig. 6 Frequency–amplitude diagrams of the first two transverse generalised coordinates of the system of Fig. 3

modal interactions and modal energy transfer, additional peaks appear in the frequency–amplitude of the p_2 .

Effects of the amplitude of the constant load position on the resonance dynamics of the beam-mass system under a moving load are highlighted in Fig. 7 for $f_m = 10.0$, $\gamma = 0.04$. For both the transverse/longitudinal motions, the overall motion amplitude is larger for larger position amplitudes; hence, the peak nonlinear resonance occurs at larger frequencies. Additionally, it is seen that the modal interactions become stronger at larger values of s_f leading to extra peaks and bifurcation points.

Shown in Fig. 8 are the force–amplitude diagrams of the moving-load-caused coupled nonlinear dynamics of

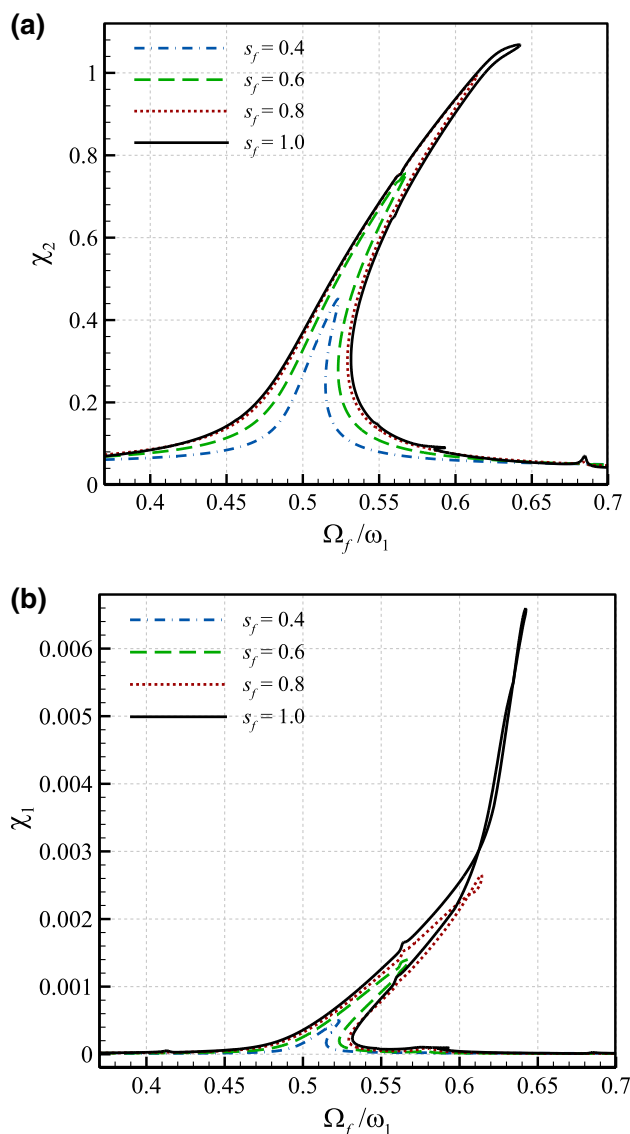


Fig. 7 Effect of the parameter s_f on frequency–amplitude diagrams of the moving-load excited beam; **a** maximum χ_2 at $\xi = 0.5$; **b** maximum χ_1 at $\xi = 0.66$. $f_m = 10.0$, $\gamma = 0.04$, $\omega_1 = 21.3204$

the beam-mass system for $\Omega_f/\omega_1 = 0.59$, $\gamma = 0.04$, $s_f = 1.0$, $\omega_1 = 21.3204$. The system initially displays two saddle-node bifurcations at $f_m = 17.68$ and 8.70 , which are the results of internal modal interactions; Fig. 9 illustrates the strong modal energy transfer in the vicinity of these two bifurcation points, leading to strong energy transfer from mode 1 to mode 2 which in turn results in a sudden local increase in second mode’s amplitude. Returning to Fig. 8, by further increasing the moving-load magnitude, the beam-mass system displays two torus bifurcations at $f_m = 32.59$ and 41.70 . Increasing the moving-load magnitude slightly further, a saddle-node bifurcation occurs at $f_m = 41.87$ causing the system to lose stability and jump to a larger-amplitude stable

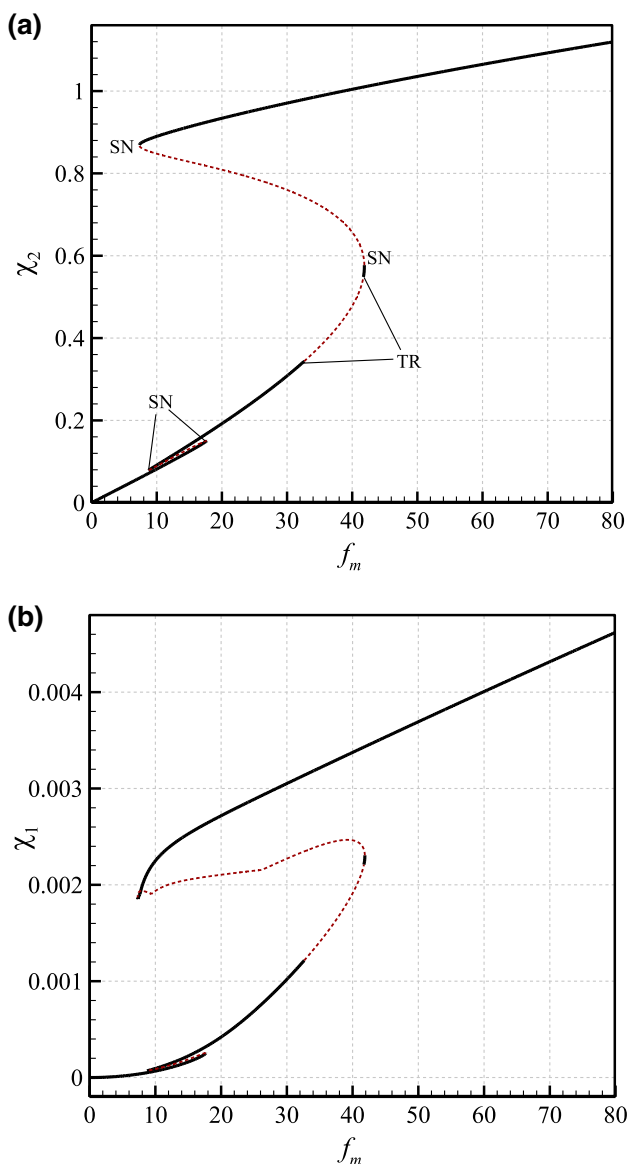


Fig. 8 Force–amplitude diagrams of the moving-load excited beam; **a** maximum χ_2 at $\xi=0.5$; **b** maximum χ_1 at $\xi=0.66$. $\Omega_f/\omega_1=0.59$ $\gamma=0.04$, $s_f=1.0$, $\omega_1=21.3204$

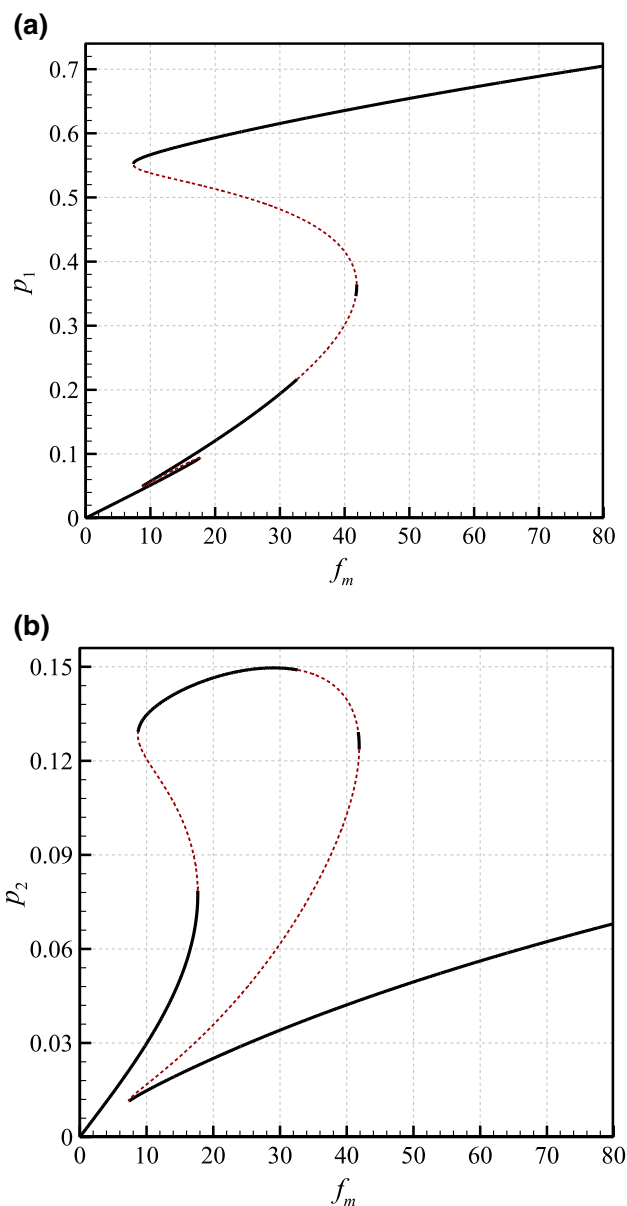


Fig. 9 Force–amplitude diagrams of the first two transverse generalised coordinates of the system of Fig. 8

limit-cycle. In all the sub-figures of Figs. 8 and 9, similar to the case of Fig. 8a, the saddle-node bifurcations are responsible for these jumps as the solution branch becomes unstable and there is no way for the system rather than jumping to the closest stable branch.

The purpose of presenting the plots of Fig. 10 is to show how different the frequency–amplitude diagrams in the moving-load-caused nonlinear dynamics of the system are to those of dynamic force with a constant position. Interestingly, the first nonlinear resonance occurs in the vicinity of the frequency ratio of 0.25 and the second in the vicinity of 0.5, third one 0.6, fourth one 0.9, then fifth around 1, and 1.35 and 1.4 for the last two one; all of them, if sufficiently

large, are hardening type. To better illustrate the contribution of each generalised coordinate to the resonance response of the beam-mass system under a moving load, Fig. 11 is constructed showing the frequency–amplitude diagrams for the first three transverse modes. As seen, the first mode reaches its peak amplitude in the vicinity of the frequency ratio of 0.5. For the second generalised coordinate, the peak amplitude occurs around $\Omega_f/\omega_1=1.0$; this ratio is 1.4 for the third generalised coordinate. This figure highlights the significant contributions of higher modes to the nonlinear dynamical response of the beam-mass system under a moving load. Hence, to study the nonlinear dynamical response

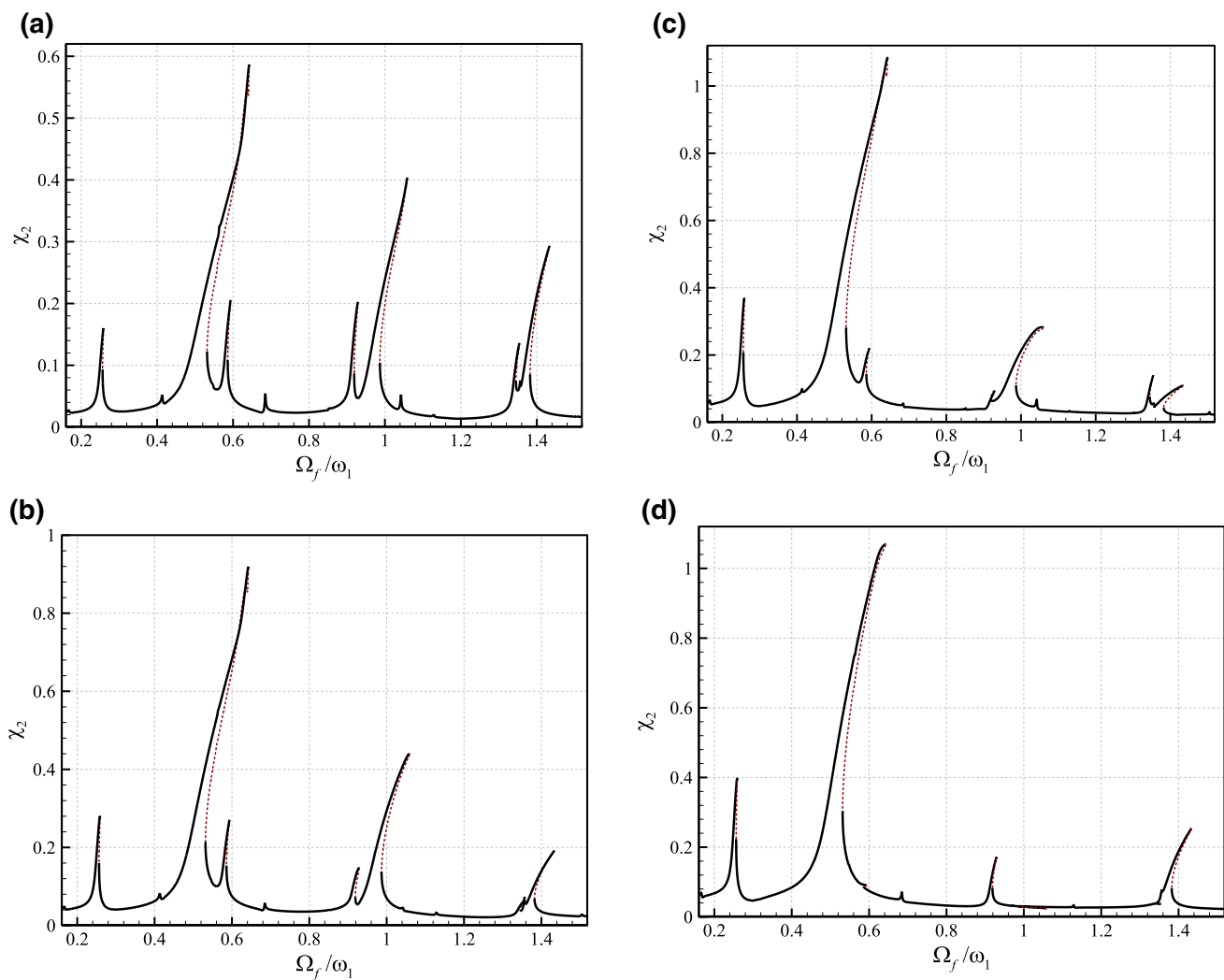


Fig. 10 Wideband frequency–amplitude diagrams of the moving-load excited beam; **a–d** the maximum transverse displacement at $\xi=0.2, 0.3, 0.4$ and 0.5 , respectively. $f_m=10.0$, $\gamma=0.04$, $s_f=1.0$, $\omega_1=21.3204$

of a system with a moving load accurately, it is essential to consider many modes in the discretisation procedure.

Depicted in Fig. 12 are the transverse/longitudinal motions for several mass ratio parameters. As seen, increasing the mass ratio causes a shift in the resonance region to the left. Additionally, the peak transverse oscillation amplitude increases as the mass ratio is increased. The nonlinear behaviour of the system seems not to be influenced by varying the mass ratio.

5 Conclusions

The moving-load-caused nonlinear coupled dynamics of beam-mass systems has been investigated. The moving load considered is of a constant magnitude which changes position harmonically. Energy stored in the beam after deflection

and the beam-mass kinetic energy were formulated. A virtual work formulation was used for the energy contribution of the moving load. The discretised equations of the beam-mass system with 20 degree of freedom were numerically integrated via continuation/time-integration techniques. A linear natural frequency verifications in the presence of point mass was performed using the FEA.

It was found that once the frequency of the force position approaches half the system's first transverse natural frequency, the system reaches its peak nonlinear resonance showing two saddle-node bifurcations. Additional saddle-node bifurcations were displayed by the system as a result of modal energy transfer and interactions. Symmetry-breaking and travelling-type motion were also displayed by the beam-mass system. Regarding the force–amplitude diagrams of the beam-mass system, there are two torus bifurcations apart from the two main saddle-node bifurcations.

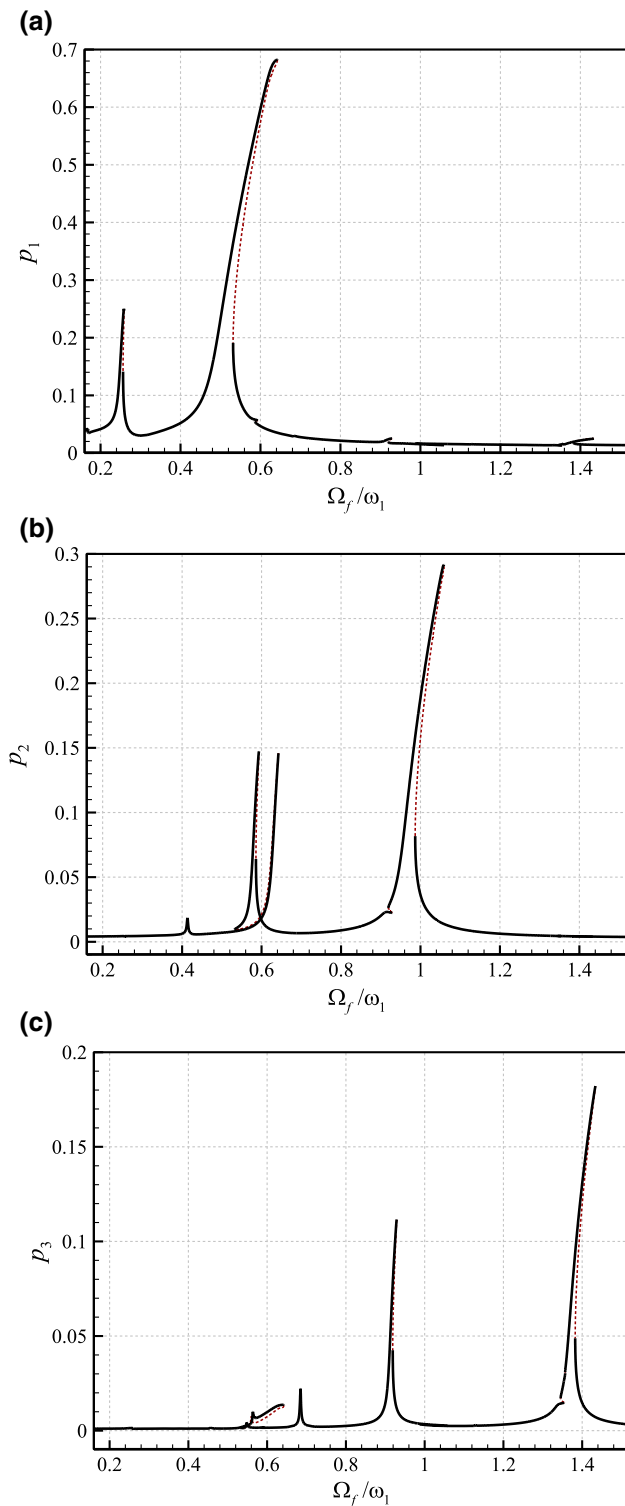


Fig. 11 Wideband frequency–amplitude diagrams of the first three transverse generalised coordinates of the system of Fig. 10

Frequency–amplitude diagrams for a wider range of frequency sweep showed that the first nonlinear resonance takes place in the vicinity of the frequency ratio of 0.25.

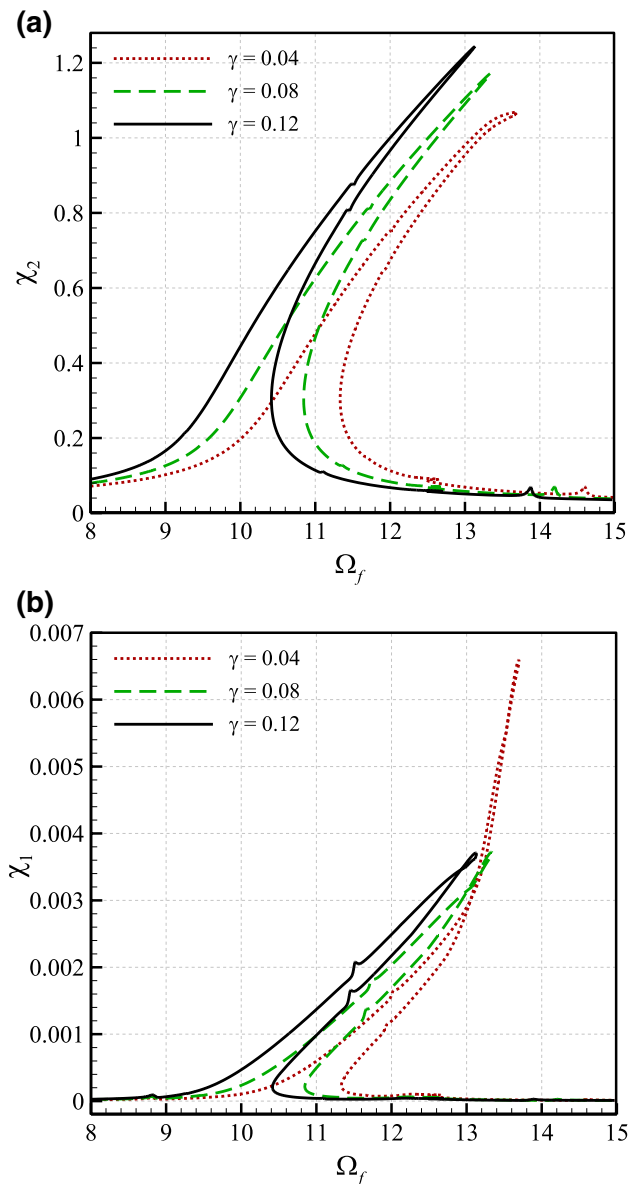


Fig. 12 Effect of the parameter γ on frequency–amplitude diagrams of moving-load excited beam; **a** maximum χ_2 at $\xi=0.5$; **b** maximum χ_1 at $\xi=0.66, f_m=10.0$

Additionally, it was shown that the peak oscillation amplitude for the first three transverse generalised coordinates occurs near frequency ratio of 0.5, 1.0, and 1.4, respectively. Examining the effect of the mass ratio showed that increasing the mass ratio results in an increase in the peak resonance transverse amplitude but does not affect the nonlinear characteristics much.

References

- Polus Ł, Szumigala M. An experimental and numerical study of aluminium–concrete joints and composite beams. *Arch Civil Mech Eng*. 2019;19:375–90.
- Domagalski Ł. Free and forced large amplitude vibrations of periodically inhomogeneous slender beams. *Arch Civil Mech Eng*. 2018;18:1506–19.
- Mohanty A, Prasad Varghese M, Kumar BR. Coupled nonlinear behavior of beam with a moving mass. *Appl Acoust*. 2019;156:367–77.
- Dimitrovová Z. Complete semi-analytical solution for a uniformly moving mass on a beam on a two-parameter visco-elastic foundation with non-homogeneous initial conditions. *Int J Mech Sci*. 2018;144:283–311.
- Esen I. Dynamic response of a functionally graded Timoshenko beam on two-parameter elastic foundations due to a variable velocity moving mass. *Int J Mech Sci*. 2019;153–154:21–35.
- Roy S, Chakraborty G, DasGupta A. On the wave propagation in a beam-string model subjected to a moving harmonic excitation. *Int J Solids Struct*. 2019;162:259–70.
- Yang D-S, Wang C. Dynamic response and stability of an inclined Euler beam under a moving vertical concentrated load. *Eng Struct*. 2019;186:243–54.
- Yang Y, Kunpang K, Lam C, Iu V. Dynamic behaviors of tapered bi-directional functionally graded beams with various boundary conditions under action of a moving harmonic load. *Eng Anal Boundary Elem*. 2019;104:225–39.
- Sarparast H, Ebrahimi-Mamaghani A. Vibrations of laminated deep curved beams under moving loads. *Compos Struct*. 2019;226:111262.
- Farokhi H, Ghayesh MH. Nonlinear motion characteristics of microarches under axial loads based on modified couple stress theory. *Arch Civil Mech Eng*. 2015;15:401–11.
- Sitar M, Kosel F, Brojan M. Large deflections of nonlinearly elastic functionally graded composite beams. *Arch Civil Mech Eng*. 2014;14:700–9.
- Pradhan KK, Chakraverty S. Static analysis of functionally graded thin rectangular plates with various boundary supports. *Arch Civil Mech Eng*. 2015;15:721–34.
- Toscano CR, Simões FMF, da Costa PA. Moving loads on beams on Winkler foundations with passive frictional damping devices. *Eng Struct*. 2017;152:211–25.
- Chen Y, Fu Y, Zhong J, Tao C. Nonlinear dynamic responses of fiber-metal laminated beam subjected to moving harmonic loads resting on tensionless elastic foundation. *Compos B Eng*. 2017;131:253–9.
- Zupan E, Zupan D. Dynamic analysis of geometrically non-linear three-dimensional beams under moving mass. *J Sound Vib*. 2018;413:354–67.
- Khurshudyan AZ, Ohanyan SK. Vibration suspension of Euler-Bernoulli-von Kármán beam subjected to oppositely moving loads by optimizing the placements of visco-elastic dampers. *ZAMM-Journal of Applied Mathematics and Mechanics/Zeitschrift für Angewandte Mathematik und Mechanik*. 2018;98:1412–9.
- Farokhi H, Ghayesh MH, Hussain S. Large-amplitude dynamical behaviour of microcantilevers. *Int J Eng Sci*. 2016;106:29–41.
- Ghayesh MH. Dynamical analysis of multilayered cantilevers. *Commun Nonlinear Sci Numer Simul*. 2019;71:244–53.
- Ghayesh MH, Farokhi H, Gholipour A, Tavallaeinejad M. Nonlinear bending and forced vibrations of axially functionally graded tapered microbeams. *Int J Eng Sci*. 2017;120:51–62.

Publisher's Note Springer Nature remains neutral with regard to jurisdictional claims in published maps and institutional affiliations